RESEARCH PAPER

CrossMark

Selective detection of copper ion in complex real samples based on nitrogen-doped carbon quantum dots

Li Zhao[1] · Huiyu Li[1] · Yuan Xu[1] · Haochi Liu[1] · Tianyu Zhou[1] · Ning Huang[1] · Yi Li[2] · Lan Ding[1]

Abstract

Highly selective nitrogen-doped carbon quantum dots (ND-CQDs) for copper ion (Cu^{2+}) determination were synthesized by a solvent-free pyrolysis of citric acid and histidine. The resultant ND-CQDs display a stable bright blue fluorescence with a satisfactory product yield of 56% and quantum yield of 16%. The ND-CQDs not only show good photostability under continuous UV irradiation, but are also dramatically stable against extreme ionic strengths. The solid powders of the ND-CQDs re-dispersed in water still maintain a strong blue fluorescence after storing at room temperature for 6 months. The ND-CQDs can be employed to selectively detect Cu^{2+} in a wide linear range of 0.6–30 μM. The detection limit is as low as 0.19 μM. The ND-CQDs were applied for Cu^{2+} detection in environmental water samples, fruit juice samples, and urine sample. Satisfactory recoveries of 96–102% with relative standard deviations below 3% were obtained. The research provided a promising prospect for selective detection of Cu^{2+} in the complex matrix.

Keywords Solid-phase method · Fluorescent detection · Selectivity · Cu^{2+} · Large scale

Introduction

Copper ion (Cu^{2+}), as a cofactor of numerous enzymes in organisms, plays a significant role in physiological and pathological fields. Excessive levels of Cu^{2+} in the human body may give rise to miscellaneous diseases, such as Wilson disease, prion disease, and Parkinson's disease [1, 2]. Hence, it is imperative to develop high-performance selective strategies for Cu^{2+} detection.

Up to now, many detection methods have been established to detect Cu^{2+}, like inductively coupled plasma mass spectrometry, inductively coupled plasma atomic emission spectrometry, and atomic absorption spectrometry. Although the aforementioned methods have high selectivity, they often require tedious

✉ Lan Ding
dinglan@jlu.edu.cn

1 College of Chemistry, Jilin University, Changchun 130012, Jilin, China

2 State Key Laboratory of Inorganic Synthesis and Preparative Chemistry, College of Chemistry, Jilin University, Changchun 130012, Jilin, China

operation and expensive instruments; more importantly, they cannot implement real-time monitoring. Fluorescent methods have attracted great attention for detection of Cu^{2+} due to the merits of low cost, fast analysis, simple operation, and real-time monitoring. In recent years, many fluorescence materials including semiconductor quantum dots [3–6], organic dyes [7, 8], and rare earth elements [9] have been developed for detecting Cu^{2+}. Nevertheless, the making of fluorescence materials from metals and highly toxic chemicals always restrict their application. Therefore, it is urgent to synthesize low-toxic fluorescence materials with fast fabrication.

As a rising star of carbon materials, carbon quantum dots (CQDs) exhibit remarkable advantages in tiny size, stable chemical inertness, and low toxicity [10–12]. Plenty of attention has been focused on detecting Cu^{2+} based on CQDs. Hou et al. [13] designed $CQDs/Zn(OH)_2$ composites for Cu^{2+} detection via encapsulating fluorescence CQDs into $Zn(OH)_2$ nanosheets, but required appropriate masking agents for Hg^{2+}. Jiang's group [14] prepared cyclam-functionalized CQDs for Cu^{2+}; the detection of Cu^{2+} was also influenced by Fe^{3+} obviously. The CQDs for high sensitive detection of Cu^{2+} have been prepared via concentrated acid reoxidized graphene oxide and activated carbon [15, 16]. The use of concentrated acid during the synthetic process is harmful to the environment. A number of researchers reported biomass materials to fabricate CQDs for sensitive detection of Cu^{2+}, while

 Springer

the synthesis of CQDs is a complex multi-step process [17–19]. Functional CQDs such as CQDs-BSA-Lys [20] and CQDs-TPEA [21] were selective for Cu^{2+} determination, but the process of further decoration is tedious. The CQDs loaded on the surface of gold nanoparticles were performed to detect Cu^{2+} while the high cost is a problem [2, 22]. It is essential to develop a simple, direct, and interference-resistant method for selective detection of Cu^{2+} based on CQDs.

In this report, a low-cost, simple, and solid-phase method was adopted to prepare stable fluorescent emissive ND-CQDs. Citric acid was selected as carbon source due to its wide application, low cost, and easy carbonation. There are a lot of reporters designed Cu^{2+} coupled CQDs as fluorescent probe for the determination of histidine on account of the excellently specific response between histidine and Cu^{2+} [23, 24]. Inspired by the ideas, the histidine was adopted as nitrogen source. There is no acid/alkali/organic solvent required during the synthesis process, which is friendly to environment. The preparation conditions of the ND-CQDs were optimized based on quantum yield (QY), product yield (PY), and determination potential of Cu^{2+}. It was delightful that the ND-CQDs without post-modification show considerable selectivity to Cu^{2+} in aqueous solution. The possible mechanism of detecting Cu^{2+} by the ND-CQDs was briefly discussed in this report. We reasoned that the surface-doped nitrogen of the ND-CQDs might induce the selective response to Cu^{2+}. The alone pairs on the nitrogen atom may play a key role in detection of Cu^{2+} via sharing electron pairs. More importantly, the ND-CQDs not only show good selectivity to Cu^{2+} in aqueous solution, but also can be utilized to detect Cu^{2+} in the practical samples with complex matrix.

Experimental

Materials

Citric acid (CA), histidine (His), and other amino acids (methionine, tryptophan, tyrosine, threonine, lysine, cysteine, aspartate, arginine, valine, leucine, phenylalanine, proline) were purchased from Sigma-Aldrich Corp. $CuCl_2$, $ZnCl_2$, $MgCl_2$, $BaCl_2$, $CdCl_2$, $FeCl_3$, $HgCl_2$, $Co(NO_3)_2 \cdot 6H_2O$, $NiCl_2$, $PbCl_2$, $CaCl_2$, $MnCl_2$, and $CrCl_3$ were supplied from Beijing Chemical Corporation (Beijing, China). Stock solutions of metal ions were obtained by dissolving relevant metal salts in deionized water. Ultrapure water with the resistivity of 18.2 MΩ cm was produced from the Milli-Q purification system (Millipore, USA).

Instruments

Transmission election microscope was used to characterize the morphology of the ND-CQDs (TEM, JEM-2100, JEOL, Japan). Nicolet 360 Fourier-transform infrared (FT-IR) spectrometer

was utilized to validate the structural features. The ESCALab 220i-XL X-ray photoelectron spectrometer was used to analyze the chemical constitution of the ND-CQDs (XPS, Thermo Electron, USA). The UV-2550 spectrophotometer (Shimadzu, Japan) was utilized to examine the UV-Vis absorption spectra, and the F-2700 fluorescence spectrophotometer (Hitachi, Japan) was used to record the fluorescence spectra.

Preparation of the ND-CQDs

The ND-CQDs were fabricated by solid-phase thermal treatment of CA and His. CA (4.0 g) and His (2.0 g) were dissolved in 10 mL of distilled water to form a transparent solution, then placed in 80 °C water bath to evaporate solvent, and got light yellow syrup product. The product was thermal-treated through a tubular furnace at 220 °C with a full of nitrogen for 120 min. The heating rate was set to 10 °C min^{-1}. Then, the brown solid product labeling as ND-CQDs was achieved and dissolved with deionized water at a concentration of 2 mg mL^{-1}. Finally, the solution was purified with a 1000-Da dialysis bag and the inside solution was collected for further applications.

As a comparison, the CA (4.0 g) and His (2.0 g) powders mixed immediately in an agate mortar, then installed in tubular furnace. The mixture was heated at 220 °C for 120 min under a continuous nitrogen atmosphere. The heating rate was set to 10 °C min^{-1}. The light brown product was achieved labeling as ND-CQDs-1.

Fluorescent detection for Cu^{2+}

xA 50 μL of the ND-CQDs (2 mg mL^{-1}) and different concentration solution of Cu^{2+} were transferred to a centrifugal tube. The mixture were diluted to 4.0 mL with NaAc-HAc buffer (pH = 4, 0.3 M), mixed thoroughly, and stored at 4 °C for fluorescent detection. The fluorescence emission spectra were examined from 300 to 600 nm with an excitation wavelength in the range of 300–400 nm. The slit of excitation and emission was 10 nm.

Pretreatment of samples

To evaluate the feasibility of the ND-CQDs for detecting Cu^{2+} in practical samples, the method was used for analysis environmental water samples, fruit juice samples, and urine sample.

Environmental water samples were acquired from Songhua river and Jingyue pond (Changchun, China). Peach juice and grape juice samples were purchased from local market in Jilin University (Changchun, China). The urine sample was acquired from a healthy volunteer in Jilin University (Changchun, China). The aforementioned samples were all filtered through 0.45-μm membrane to remove large particles prior to the fluorescent detection and fruit juice samples were further diluted 20-fold with distilled water.

Scheme 1 Schematic illustration of the preparation of the ND-CQDs and its detection mechanism to Cu²⁺
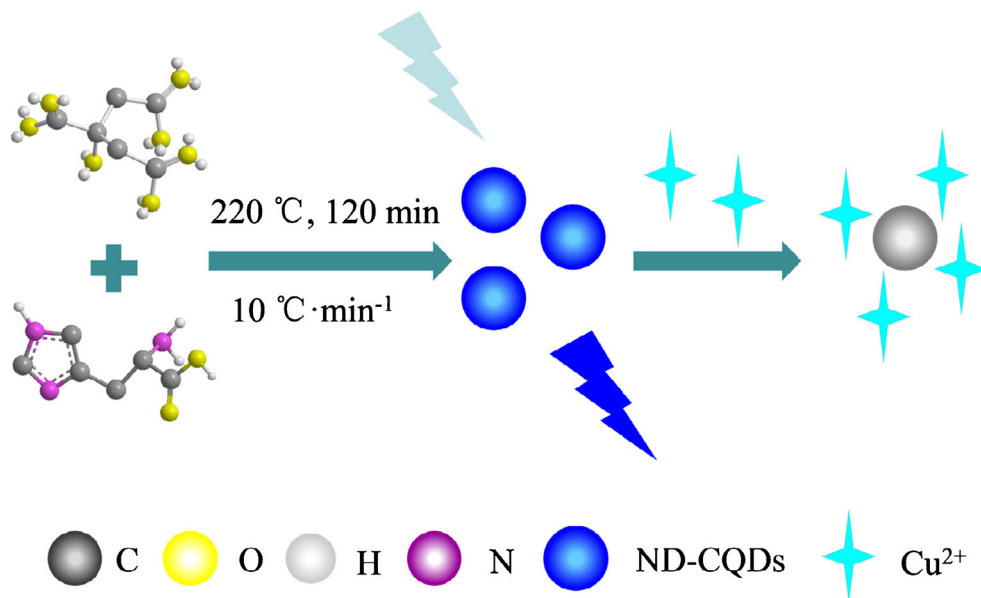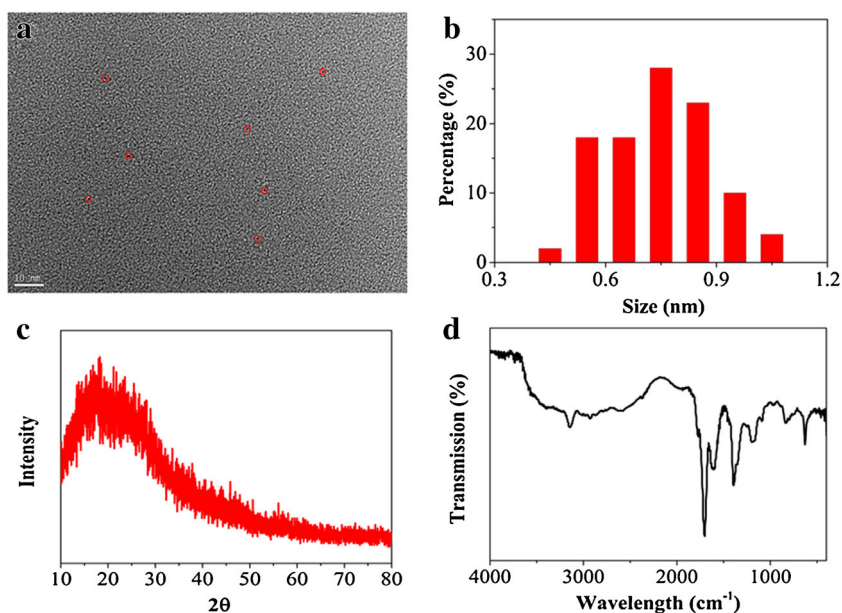

Results and discussion

### The optimization of preparation conditions

The blue emissive ND-CQDs were prepared via a solvent-free method with CA and His as starting materials, as illustrated in Scheme 1. The evolution of QY and PY was investigated to optimize synthetic conditions of reaction temperature, reaction time, and ratios of regents. As shown in Fig. S1a (see Electronic Supplementary Material, ESM), when the temperature is below 220 °C, the fluorescent QY increases from 2.4 to 16% and PY increases from 15 to 56% as the rising of reaction temperature. Fluorescent QY and PY distinctly reduce to 2.9 and 13% when the temperature increases to

240 °C. The influence of reaction time is similar to the reaction temperature. As illustrated in Fig. S1b (see ESM), with the increase of reaction time, the maximum QY of 16% and PY of 56% can be obtained at 120 min. The excessive carbonization may ruin carbon skeleton leading to fluorescence intensity reduction [25]. The ratio of CA and His (w/w) varying from 4:1 to 1:1 was also studied. The results in Fig. S1c (see ESM) demonstrate the ND-CQDs with the maximum QY of 16% and PY of 56% can be acquired when the ratio of CA and His is 2:1. It is worthy to mention that the ND-CQDs have a much higher QY and PY than both of the CA-CQDs and the His-CQDs, which the CA-CQDs only using CA as carbon source and the His-CQDs only employing His as precursor were prepared in the same manner of the ND-CQDs, respectively. The QY and PY of

Fig. 1 TEM (a) and size distribution (b) of the ND-CQDs; XRD (c) and FT-IR (d) of the ND-CQDs
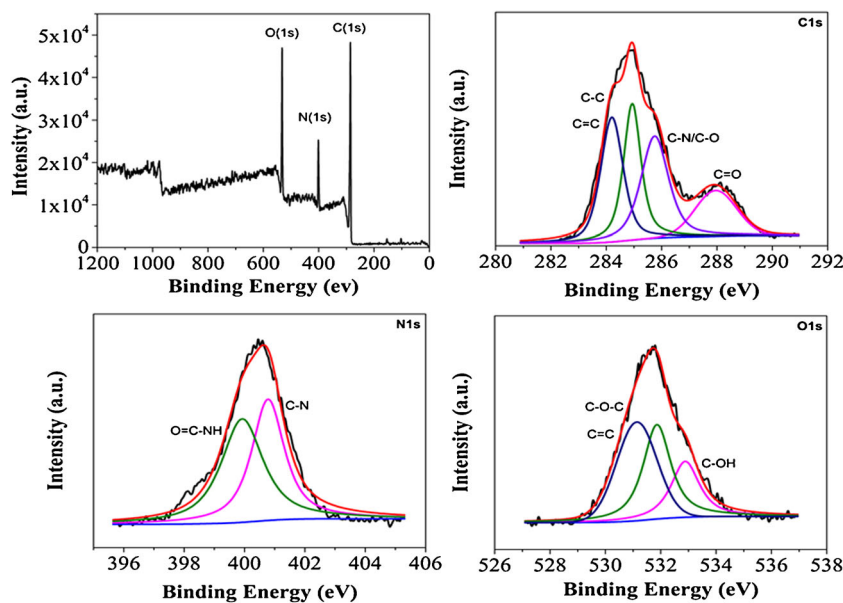
the CA-CQDs are determined to be 4.7 and 12% and the His-CQDs are 10 and 20%, respectively.

In order to illustrate the influence of mixed mode of CA and His on QY and PY of the ND-CQDs, a contrast experiment of CA and His in powder mixed immediately was performed. For ND-CQDs-1, the QY and PY, which are calculated to be 2.3 and 11%, are much lower than that of ND-CQDs. Compared to the means of mixing directly, the way of dissolving CA and His in distilled water is much easier to form a more uniform mixture between CA and His. As a result, it is more favorable for His, as a nitrogen source, to take part in the synthesis of the ND-CQDs. That may be the reason for the enhancement of both QY and PY.

The optimal synthetic conditions were selected as follows: dissolving CA and His in deionized water to form a homogeneous mixture, 220 °C for 120 min with a continuous flow of nitrogen for carbonization, and 2:1 of the ratio for CA:His.
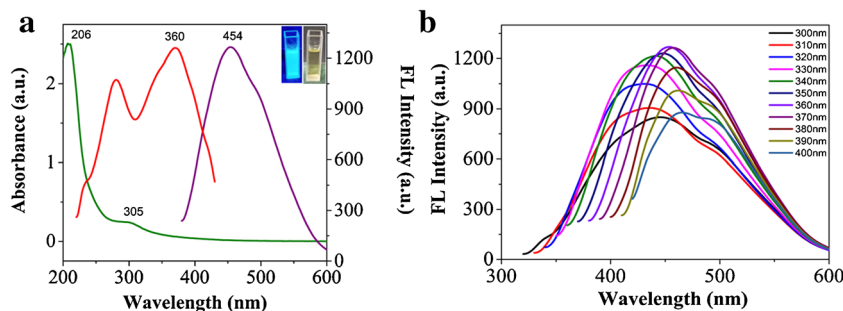
Characterization and properties of the ND-CQDs

TEM was used to evaluate the morphology of the ND-CQDs. As demonstrated in Fig. 1a, the ND-CQDs are almost spherical with the average diameter of 0.74 nm. Figure 1b shows a narrow size distribution from 0.35 to 1.04 nm. The XRD in Fig. 1c

exhibits a broad peak at $2\theta = 18°−25°$, indicating a highly disordered carbon species. The FT-IR spectrum is presented in Fig. 1d. The weak peak at around 3400 cm^{-1} belongs to the vibration of O–H. The bond around 3143 cm^{-1} corresponds to the vibration of N–H. Characteristic peaks at 1701 and 1611 cm^{-1} represent the typical stretching vibrations of C–O and CO–NH [26, 27]. The bond at 1393 cm^{-1} can be relevant to the skeletal vibration of the heteroatomic ring [28]. The peak at 1185 cm^{-1} implies the existence of C–O–C group. These results imply that the ND-CQDs possess many hydrophilic functional groups containing amino, hydroxyl, and carboxyl groups. The findings indicate that the ND-CQDs show a great potential in aqueous phase analysis without further decoration.

XPS was used to further confirm the structure information of the ND-CQDs. The full spectrum in Fig. 2 exhibits three prominent features of C1s at 284.9 eV, N1 s at 531.7 eV, and O1s at 400.5 eV, with atomic percentages of 69.6, 12.2, and 18.2%, respectively. The content of nitrogen is higher than reported [29, 30], which may result from forming a homogeneous mixture by premixing CA and His in deionized water. The C1s spectrum can be resolved into four peaks corresponding to –C–C (284.2 eV), –C–C (284.9 eV), C–O/C–N (285.7 eV), and –C–O (287.9 eV) groups, respectively [31, 32]. Reviewing the N1s

Fig. 4 **a** Fluorescence intensity of the ND-CQDs at different concentration NaCl from 0.1 to 1.0 M (pH = 4). **b** The effect of pH on fluorescence intensity of the ND-CQDs in the absence and presence of Cu^{2+} (the concentration of Cu^{2+} is 30 μM)
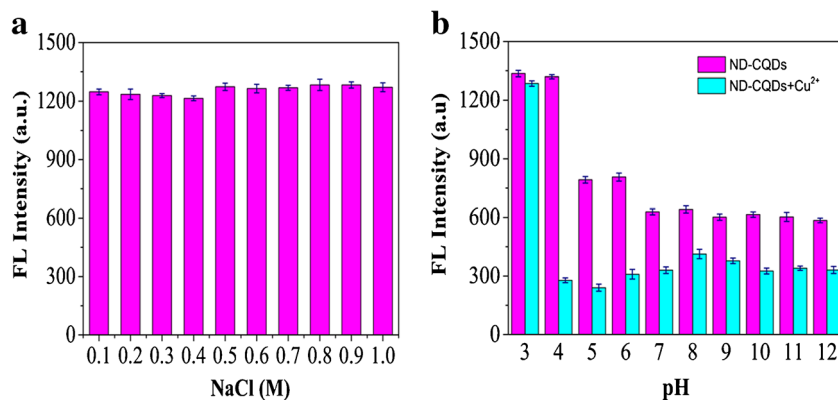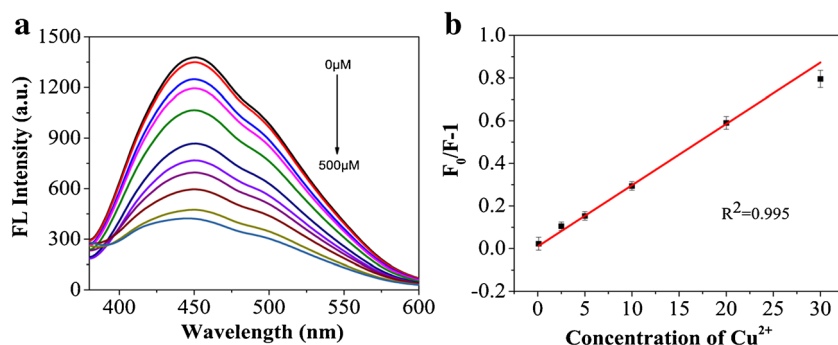

spectrum of two components at 399.9 and 400.8 eV, they are assigned to O–C–NH and –C–N– functional groups, respectively [26]. The O1s spectrum displays three distinct peaks which assign to –C–O (531.1 eV), –C–O–C (531.9 eV), and –C–OH (532.8 eV) groups, respectively [31, 33].

Optical properties of the ND-CQDs

The optical properties including UV-Vis absorption and emission/excitation spectra of the ND-CQDs were further explored. As exhibited in Fig. 3a, the ND-CQD aqueous solution displays two obvious absorption peaks at 206 and 305 nm. The former is ascribed to π–π* transitions and the latter belongs to n–π* transitions by the surface states [23, 34]. The ND-CQD aqueous solution is yellowish in color under daylight and displays distinct blue luminescence under UV excitation (inset of the Fig. 3a). As described in Fig. 3b, the emission spectrum of the ND-CQDs is broad and excitation-dependent. The ND-CQDs show a maximum emission wavelength of 454 nm when excited at 360 nm. The phenomenon of the excitation-dependence is associated with the particles of diverse size and a distribution of different energy traps by different surface states. By employing quinine sulfate in sulfuric acid (0.1 M, QY = 0.54) as a standard, the QY of 16% (λ = 360 nm) is computed by the subsequent equation:

$$Y_u = Y_s \frac{F_u}{F_s} \frac{A_s}{A_u} \qquad (1)$$

where Y is the QY and the subscripts u and s signify the ND-CQDs and quinine sulfate. F and A denote integral fluorescence intensity and UV absorption value at maximum excitation wavelength of 360 nm, respectively.

Fluorescent stability of the ND-CQDs

Subsequently, the effects of ionic strength, concentration of salt, pH, and continuous UV exposure on fluorescent stability of the ND-CQDs were detected. In view of Fig. 4a, there is nearly no variation in fluorescence intensity at different NaCl concentrations (0.1–1.0 M, pH = 4). As described in Fig. 4b, pH has a noticeable impact on fluorescent intensity of the ND-CQDs. The ND-CQDs show strong fluorescent intensity under the condition of acid. The fluorescent intensity reduces gradually with the increase of the pH. The quenching efficiency is the highest when the optimum pH is 4 that may relate to the surface state of the ND-CQDs. When continuously exposing under UV light for 90 min, the fluorescence intensity of the ND-CQDs is decreased to pristine 87% (ESM Fig. S2). The phenomenon suggests that the ND-CQDs have good resistance to light bleaching performance. As exhibited in Fig. S3 (see ESM), the solid powders of the ND-CQDs, storing at room temperature for 6 months, not only can be re-dispersed in water homogeneously, but also exhibit strong blue fluorescence. By taking the advantages of stability, the ND-CQDs are available in real sample determination.

Fig. 5 **a** The fluorescence spectrum of the ND-CQDs with different concentrations of Cu^{2+} in the range of 0–500 μM. **b** The relationship between $F_0/F - 1$ and the concentration of Cu^{2+} (F_0 and F are the fluorescent intensity of the ND-CQDs in the absence and presence of Cu^{2+})

Fig. 6 Fluorescence response of the ND-CQDs to metal ions (**a**) and amino acids (**b**) (the concentration of Cu^{2+} is 30 μM; other metal ions and amino acids are 3 mM)
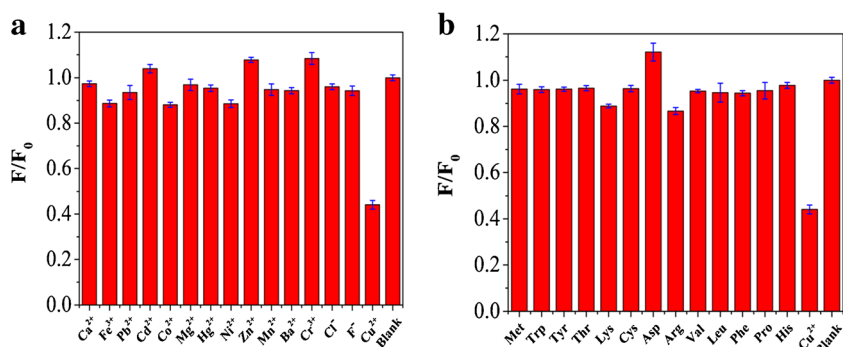
Fluorescent detection of Cu^{2+}

It was found that the ND-CQDs show high affinity to Cu^{2+} during the experiments, so a series of the fluorescent experiments were performed. As shown in Fig. 5a, the variation behavior of fluorescence quenching efficiency at 360 nm by increasing the concentration of Cu^{2+} can be observed. The relationship of fluorescence quenching efficiency ($F_0/F-1$) and Cu^{2+} concentration is illustrated by the Stern-Volmer equation, and the equation is presented as follows:

$$F_0/F = 1 + K_{sv}C \qquad (2)$$

F_0 signify the initial fluorescence intensity. F is the fluorescence intensity after adding Cu^{2+} into ND-CQD solution. K_{sv} is the quenching constant. C represents the concentration of Cu^{2+}. As described in Fig. 5b, the result reveals that the fluorescence intensity ratio ($F_0/F-1$) is linearly relevant to the concentration of Cu^{2+} in the detection range of 0.6–30 μM ($R^2 = 0.995$). The limit of detection (LOD) is calculated to be 0.19 μM (S/N = 3).

In the sensing system, selectivity was taken out to explore the applicability of the ND-CQDs for Cu^{2+} determination. As exhibited in Fig. 6a, the results indicate that the ND-CQDs show a highest selectivity for Cu^{2+} determination among the other mental ions like Ca^{2+}, Fe^{3+}, Pb^{2+}, Cd^{2+}, Co^{2+}, Mg^{2+}, Hg^{2+}, Ni^{2+}, Zn^{2+}, Mn^{2+}, Ba^{2+}, and Cr^{3+}. The result in Fig. 6b reveals that the tested amino acids (Met, Trp, Tyr, Thr, Lys, Cys, Asp, Arg, Val, Leu, Phe, Pro, His) have negligible influence on Cu^{2+} determination by the ND-CQDs.

The fluorescence quenching mechanism of ND-CQDs by Cu^{2+} was studied. We speculated that the fluorescent quenching phenomenon was the result from the interaction between Cu^{2+} and the nitrogen-containing groups on the surface of the ND-CQDs. To prove this assumption, the experiments of the CA-CQDs and the His-CQDs were performed. In Fig. S4a (see ESM), the CA-CQDs show a similar emission wavelength at 450 nm ($\lambda = 360$ nm) to that of the ND-CQDs. His-CQDs display a maximum emission wavelength at 437 nm ($\lambda = 360$ nm), which is blue-shift 20 nm approximately than that of the ND-CQDs (ESM Fig. S4b). Fluorescence response of the CA-CQDs and the His-CQDs to tested metal ions were evaluated as well (Fig. 7). The CA-CQDs show no response to Cu^{2+} while the His-CQDs can respond to numerous metal ions.

It is well known that the functional groups have a significant effect on the fluorescent behavior of CQDs. FT-IR analysis was performed to examine the surface functional groups of the CA-CQDs and the His-CQDs. As depicted in Fig. S5 (see ESM), the CA-CQDs display an obvious peak at 1778 cm^{-1} assigning to carboxyl, which may be the reason for special response to Fe^{3+} rather than Cu^{2+}. In view of ND-CQDs, the peak of carboxyl is weakened. The appearance of characteristic peak of amide bond at 1701 and 1611 cm^{-1} proves that surface-doped nitrogen of the ND-CQDs can be the reason for selectively detecting Cu^{2+}. Compared to the ND-CQDs, the His-CQDs show various functional groups correlating to the peaks around 2021 to 845 cm^{-1}, which offered more binding sites to many metal ions and led to a loss of selectivity.

Fig. 7 Fluorescence response of the CA-CQDs (**a**) and the His-CQDs (**b**) aqueous solution to various metal ions (the concentrations of metal ions are 30 μM)
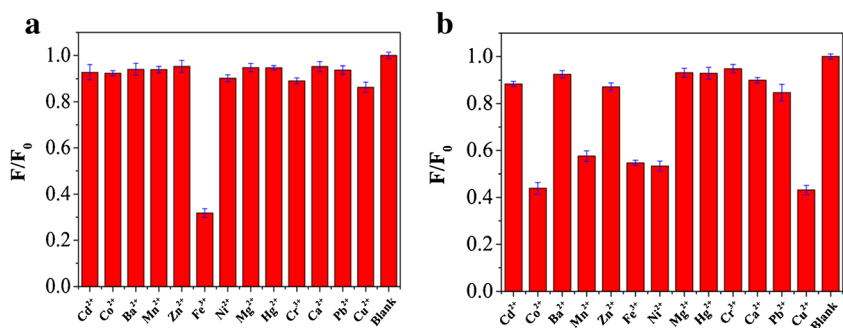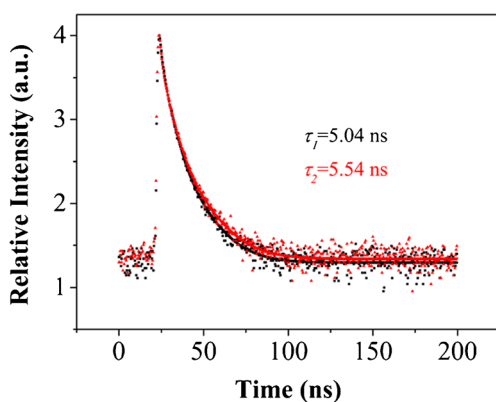
Fig. 8 Fluorescent decay curves of the ND-CQDs and ND-CQDs-Cu^{2+}

These results indicate that CA and His all take part in the synthesis of ND-CQDs, and the ND-CQDs with electron donor groups like nitrogen-containing groups donate an electron to Cu^{2+}; the alone pair on the N atom shows a favorable affinity to Cu^{2+}. The fluorescence quenching of ND-CQDs is achieved via sharing electron pairs between the N atom and Cu^{2+} [15, 17, 35].

The fluorescent lifetimes of ND-CQDs and ND-CQDs-Cu^{2+} were carried out. Fluorescent lifetime is a distinct and definitive way to distinguish whether static quenched or dynamic quenched. In Fig. 8, the fluorescent decay curve is best fitted with a bi-exponential equation as follows:

$$R_t = A_1 \exp(-t/\tau_1) + A_2 \exp(-t/\tau_2) \qquad (3)$$

where R_t is the intensity usually assuming to decay as the sum of individual single exponential decay. A is the fractional

contributions of time-resolved decay lifetime and τ is the decay time. As displayed in Fig. 8, the average fluorescent lifetime of pure ND-CQDs is 5.04 ns. When adding Cu^{2+} into the ND-CQDs solution, the average fluorescent lifetime changes to 5.54 ns. The result demonstrates that a dynamic quenching appears on the excited photon of the ND-CQDs returning to ground state through the collision between Cu^{2+} and the ND-CQDs with charge transfer.

Analysis of Cu^{2+} in practical samples

The ND-CQDs were applied to detect Cu^{2+} in practical samples. The results showed that the Cu^{2+} was not detected in the real samples and were in accordance with that detection by ICP-OES. The spiked samples were further carried out to explore the recoveries of this method. As revealed in Table 1, the satisfactory recoveries are obtained in the range of 96–102% and the RSDs are below 3% ($n = 3$), which is comparable to other reported probes in ESM Table S1 [2, 14, 15, 36–40]. The LOD of the ND-CQDs for determination of Cu^{2+} is 0.19 μM, which is far below the upper limit of copper ions in drinking water (20 μM) of the U.S Environmental Protection Agency [41].

Conclusion

In this work, a cost-efficient and simple method was adopted to prepare the ND-CQDs with CA and His as precursors. The proposed method reflects on its facile, free acid/alkali/organic solvent, and large scale compared to traditional methods for preparing CQDs. Under the optimal preparation conditions, the ND-CQDs have a narrow size distribution, stable blue fluorescence, high product yield, and quantum yield. In comparison to other reported CQDs that only applied to detect Cu^{2+} in the water environment, the ND-CQDs without post-modification in this report not only show considerable and selective response to Cu^{2+} in the aqueous solution, but also exhibit satisfactory performance for the detection of Cu^{2+} in more complex real samples, such as fruit juice samples and urine sample. The approach may pave a way for the contribution of highly selective detecting Cu^{2+} and the ND-CQDs are a promising candidate for applying in large scale.

Compliance with ethical standards

Conflict of interest The authors declare that they have no conflicts of interests.

Table 1 The results of analysis of Cu^{2+} in real spiked samples via the ND-CQDs

Samples	Spiked (μM)	Found (μM)	RSD ($n = 3\%$)	Recoveries (%)
Songhua river	10.0	10.2	2	102
	15.0	15.1	2	101
	20.0	19.5	2	98
Jingyue pond	10.0	10.1	1	101
	15.0	14.9	1	99
	20.0	19.2	1	96
Grape juice	10.0	9.8	2	98
	15.0	15.2	1	101
	20.0	19.5	1	98
Peach juice	10.0	9.8	1	98
	15.0	14.5	3	97
	20.0	19.4	1	97
Urine	10.0	10.1	2	101
	15.0	14.6	1	97
	20.0	19.6	2	98

Ethical standards and informed consent The urine sample was obtained from a healthy volunteer in Jilin University and informed consent was obtained for the use of human urine. This research was approved by Jilin University Ethic Committee and all experiments were performed in accordance with the Guideline for Experimentation of Jilin University.

References

1. Wang YH, Zhang C, Chen XC, Yang B, Yang L, Jiang CL, et al. Ratiometric fluorescent paper sensor utilizing hybrid carbon dots-quantum dots for the visual determination of copper ions. Nano. 2016;8:5977–84.

2. Shen QP, Li WH, Tang SY, Hu YF, Nie Z, Huang Y, et al. A simple "clickable" biosensor for colorimetric detection of copper(II) ions based on unmodified gold nanoparticles. Biosens Bioelectron. 2013;41:663–8.

3. Zhu AW, Qu Q, Shao XL, Kong B, Tian Y. Carbon-dot-based dual-emission nanohybrid produces a ratiometric fluorescent sensor for in vivo imaging of cellular copper ions. Angew Chem. 2012;124:7297–301.

4. Gong TT, Liu JF, Liu XX, Liu J, Xiang JK, Wu YW. A sensitive and selective sensing platform based on CdTe QDs in the presence of L-cysteine for detection of silver, mercury and copper ions in water and various drinks. Food Chem. 2016;213:306–12.

5. Han CP, Li HB. Host-molecule-coated quantum dots as fluorescent sensors. Anal Bioanal Chem. 2010;397:1437–44.

6. Li HM, Wang XF, Cai Z, Lu L, Tao J, Sun B, et al. Ratiometric fluorescent sensing of copper ion based on chromaticity change strategy. Anal Bioanal Chem. 2017;409:6655–62.

7. Liu XJ, Zhang N, Bing T, ShangGuan DH. Carbon dots based dual-emission silica nanoparticles as a ratiometric nanosensor for Cu^{2+}. Anal Chem. 2014;86:2289–96.

8. Fu HL, Ji ZY, Chen XJ, Cheng AW, Liu SC, Gong PW, et al. A versatile ratiometric nanosensing approach for sensitive and accurate detection of Hg^{2+} and biological thiols based on new fluorescent carbon quantum dots. Anal Bioanal Chem. 2017;409:2373–82.

9. Wang YR, Wang H, Zhao X, Jin YT, Xiong HQ, Yuan JL, et al. A beta-diketonate-europium(III) complex-based fluorescent probe for highly sensitive time-gated luminescence detection of copper and sulfide ions in living cell. New J Chem. 2017;41:5981–7.

10. Zheng M, Xie ZG, Qu D, Li D, Du P, Jing XB, et al. On-off-on fluorescent carbon dot nanosensor for recognition of chromium(VI) and ascorbic acid based on the inner filter effect. ACS Appl Mater Interfaces. 2013;5:13242–7.

11. Zong J, Yang XL, Trinchi A, Hardin S, Cole I, Zhu YH, et al. Carbon dots as fluorescent probes for "off–on" detection of Cu^{2+} and L-cysteine in aqueous solution. Biosens Bioelectron. 2014;51:330–5.

12. Shi YP, Pan Y, Zhang H, Zhang ZM, Li MJ, Yi CQ, et al. A dual-mode nanosensor based on carbon quantum dots and gold nanoparticles for discriminative detection of glutathione in human plasma. Biosens Bioelectron. 2014;56:39–45.

13. Hou J, Zhou TY, Wang L, Zhang P, Ding L. Template-free microwave-assisted fabrication of carbon dots/Zn(OH)$_2$ composites for separation and enhancing chemical sensing. Sensors Actuators B Chem. 2016;230:615–22.

14. Chen J, Li Y, Lv K, Zhong WB, Wang H, Wu Z, et al. Cyclam-functionalized carbon dots sensor for sensitive and selective detection of copper(II) ion and sulfide anion in aqueous media and its imaging in live cells. Sensors Actuators B Chem. 2016;224:298–306.

15. Wang FX, Gu ZY, Lei W, Wang WJ, Xia XF, Hao QL. Graphene quantum dots as a fluorescent sensing platform for highly efficient

16. detection of copper(II) ions. Sensors Actuators B Chem. 2014;190:516–22.

17. Zhang SR, Wang Q, Tian GH, Ge HG. A fluorescent turn-off/on method for detection of Cu^{2+} and oxalate using carbon dots as fluorescent probes in aqueous solution. Mater Lett. 2014;115:233–6.

17. Gedda G, Lee CY, Lin Y, Wu HF. Green synthesis of carbon dots from prawn shells for highly selective and sensitive detection of copper ions. Sensors Actuators B Chem. 2016;224:396–403.

18. Yang SW, Sun J, Li XB, Zhou W, Wang ZY, He P, et al. Large-scale fabrication of heavy doped carbon quantum dots with tunable-photoluminescence and sensitive fluorescence detection. J Mater Chem A. 2014;2:8660–7.

19. Hu C, Yu C, Li MY, Wang XN, Yang JY, Zhao ZB, et al. Chemically tailoring coal to fluorescent carbon dots with tuned size and their capacity for Cu(II) detection. Small. 2014;10:4926–33.

20. Liu JM, Lin LP, Wang XX, Lin SQ, Cai WL, Zhang LH, et al. Highly selective and sensitive detection of Cu^{2+} with lysine enhancing bovine serum albumin modified-carbon dots fluorescent probe. Analyst. 2012;137:2637–42.

21. Ting SL, Ee SJ, Ananthanarayanan A, Leong KC, Chen P. Graphene quantum dots functionalized gold nanoparticles for sensitive electrochemical detection of heavy metal ions. Electrochim Acta. 2015;172:7–11.

22. Dong YQ, Wang RX, Li H, Shao JW, Chi YW, Liu XM, et al. Polyamine-functionalized carbon quantum dots for chemical sensing. Carbon. 2012;50:2810–5.

23. Zhu XH, Zhao TB, Nie Z, Miao Z, Liu Y, Yao SZ. Nitrogen-doped carbon nanoparticle modulated turn-on fluorescent probes for histidine detection and its imaging in living cells. Nano. 2016;8:2205–11.

24. Wang Y, Qu K, Tang L, Li Z, Moore E, Zeng X, et al. Nanomaterials in carbohydrate biosensors. TrAC TendS Anal Chem. 2014;58:54–70.

25. Xia C, Hai X, Chen XW, Wang JH. Simultaneously fabrication of free and solidified N, S-doped graphene quantum dots via a facile solvent-free synthesis route for fluorescent detection. Talanta. 2017;168:269–78.

26. Wang XD, Wang D, Guo YL, Yang CD, Iqbal A, Liu WS, et al. Imidazole derivative-functionalized carbon dots: using as a fluorescent probe for detecting water and imaging of live cells. Dalton Trans. 2015;44:5547–54.

27. Zhang ZM, Shi YP, Pan Y, Cheng X, Zhang LL, Chen JY, et al. Quinoline derivative-functionalized carbon dots as a fluorescent nanosensor for sensing and intracellular imaging of Zn^{2+}. J Mater Chem B. 2014;2:5020–7.

28. Ding H, Zhang P, Wang TY, Kong JL, Xiong HM. Nitrogen-doped carbon dots derived from polyvinyl pyrrolidone and their multicolor cell imaging. Nanotechnology. 2014;25:205604.

29. Yuan FL, Wang ZB, Li XH, Li YC, Tan ZA, Fan LZ, et al. Bright multicolor bandgap fluorescent carbon quantum dots for electroluminescent light-emitting diodes. Adv Mater. 2017;29:1604436.

30. Zhang Y, Cui PP, Zhang F, Feng XT, Wang YL, Yang YZ, et al. Fluorescent probes for "off–on" highly sensitive detection of Hg^{2+} and L-cysteine based on nitrogen-doped carbon dots. Talanta. 2016;152:288–300.

31. Wang H, Sun C, Chen XR, Zhang Y, Colvin VL, Rice Q, et al. Excitation wavelength independent visible color emission of carbon dots. Nano. 2017;9:1909–15.

32. Niu XQ, Liu GS, Li LY, Fu Z, Xu H, Cui FL. Green and economical synthesis of nitrogen-doped carbon dots from vegetables for sensing and imaging applications. RSC Adv. 2015;5:95223–9.

33. Wang Y, Zhuang QF, Ni YN. Facile microwave-assisted solid-phase synthesis of highly fluorescent nitrogen-sulfur-codoped carbon quantum dots for cellular imaging applications. Chem Eur J. 2015;21:13004–11.

34. Dong YQ, Pang HC, Yang HB, Guo CX, Shao JW, Chi YW, et al. Carbon-based dots co-doped with nitrogen and sulfur for high quantum yield and excitation-independent emission. Angew Chem Int Ed. 2013;52:7800–4.

35. Zhang ZM, Pan Y, Fang YN, Zhang LL, Chen JY, Yi CQ. Tuning photoluminescence and surface properties of carbon nanodots for chemical sensing. Nano. 2016;8:500–7.

36. Liu YS, Zhao YN, Zhang YY. One-step green synthesized fluorescent carbon nanodots from bamboo leaves for copper(II) ion detection. Sensors Actuators B Chem. 2014;196:647–52.

37. Castillo AS, Morales DP, Fernández AL, Avidad MA, Castillo E, Olmos AM, et al. Evaluation of a reconfigurable portable instrument for copper determination based on luminescent carbon dots. Anal Bioanal Chem. 2016;408:3013–20.

38. Xu PP, Wang CF, Sun D, Chen YJ, Zhou KL. Ionic liquid as a precursor to synthesize nitrogen- and sulfur-co-doped carbon dots for detection of copper(II) ions. Chem Res Chin Univ. 2015;31:730–5.

39. Hua C, Zhang WH, De Almeida SRM, Ciampi S, Gloria D, Liu GZ, et al. A novel route to copper(II) detection using 'click' chemistry-induced aggregation of gold nanoparticles. Analyst. 2012;137:82–6.

40. Yetisen AK, Montelongo Y, Qasim MM, Butt H, Wilkinson TD, Monteiro MJ, et al. Photonic nanosensor for colorimetric detection of metal ions. Anal Chem. 2015;87:5101–8.

41. Donohue J. Copper in drinking-water. Geneva: World Health Organization; 1988.